Rhodium Dinitrogen Complexes $Rh(NN)_x$ ($x = 1-3$) and Anions: Matrix Infrared Spectra and DFT Calculations

Xuefeng Wang and Lester Andrews*

Department of Chemistry, University of Virginia, Charlottesville, Virginia 22904-4319

Received: September 13, 2001; In Final Form: December 4, 2001

Reactions of laser-ablated rhodium atoms with molecular nitrogen in excess neon produce the rhodium nitrogen complexes $Rh(NN)_x$ ($x = 1-3$) and their counterpart anions through the capture of ablated electrons. The observed absorption bands are identified by isotopic substitution and DFT calculations of vibrational fundamentals. The N−N stretching fundamental at 2162.0 cm^{-1} for RhNN and the antisymmetric N−N mode for $Rh(NN)_2$ at 2199.3 cm^{-1} in solid neon are in accord with earlier argon matrix assignments. Three N−N stretching frequencies at 2185.2, 2203.3, and 2235.6 cm^{-1} are assigned to $Rh(NN)_3$, which is calculated to have a T-shaped structure with a $^2A_1$ ground state. The photosensitive $Rh(NN)_x^-$ ($x = 1-3$) anions are eliminated with CCl_4 doping to capture ablated electrons.

Introduction

The chemistry of rhodium is very important in surface science and catalytic technology since the metal can easily coordinate with many organic and inorganic molecules, which are in turn very reactive and widely used both for fundamental studies in the laboratory and catalysis in industry.[1−8] For example, the supported unsaturated Rh(CO) species can activate the C−H bond in alkanes and the H−H bond in hydrogen.[6,7] Recently, the reactions of laser-ablated Rh atoms with small molecules in excess argon and neon have been investigated in this research group, and several unsaturated rhodium carbonyls and nitrosyls, as well as cations and anions have been identified.[9−13] These species are important models to understand rhodium catalyst systems. The interaction of N_2 with rhodium[1,2,4,5,8] is of particular interest here.

The bonding type of N_2 coordinated to transition metals has been an issue for many organometallic complexes with dinitrogen and for N_2 adsorption on supported metal surfaces. Both end-on (η^1) and side-on (η^2) have been investigated on metal surfaces; however, end-on bonding is more stable and much more prevalent.[14] Early thermal Rh atom matrix isolation investigations identified neutral $Rh(NN)_{1,2,3}$ complexes in solid argon and $Rh(NN)_4$ in solid nitrogen.[15] In addition, laser-ablation experiments with the rhodium and nitrogen gave rhodium nitrides RhN, Rh_2N, and Rh_2N_2 in solid argon and nitrogen.[10] We report here reactions of laser-ablated rhodium with nitrogen in excess neon, argon, and pure nitrogen, which produce neutral complexes and a small yield of rhodium dinitrogen complex anions. The vibrational frequencies of the reaction products are confirmed using isotopic substitution upon the infrared spectra and density functional (DFT) calculations. Finally, it is interesting to compare the stoichiometry of N_2 and CO complexes with a given metal. In the case of Pd and Pt, only two N_2 ligands can bind whereas tetracarbonyls are observed.[16,17] Recent studies involving sequential bond energies for $Ni(CO)_x^+$ and $Ni(N_2)_x^+$ show that the carbonyl bonds are considerably stronger.[18] Rhodium tetracarbonyl is a stable molecule, based on experiment and theory,[11] but how many N_2 ligands can attach to the naked Rh center?

* To whom correspondence should be addressed. E-mail: lsa@virginia.edu.

Experimental and Theoretical Methods

The experiment for reactions of laser-ablated metal atoms with small molecules during condensation in excess neon has been described in detail previously.[19,20] The Nd:YAG laser fundamental (1064 nm, 10 Hz repetition rate with 10 ns pulse width) was focused onto the rotating rhodium target (Goodfellow). The laser energy was varied from 1 to 20 mJ/pulse. Laser-ablated rhodium atoms were codeposited with nitrogen molecules (0.1 to 0.3%) in excess neon, argon, or pure N_2 onto a 4 K CsI window at 2−4 mmol/h for one h using a Sumitomo Heavy Industries Model RDK-205D Cryocooler. Isotopic $^{15}N_2$ and $^{14}N_2 + {}^{15}N_2$ mixtures were used in different experiments. Infrared spectra were recorded at 0.5 cm^{-1} resolution on a Nicolet 750 with 0.1 cm^{-1} accuracy using an MCTB detector. Matrix samples were annealed at different temperatures, and selected samples were subjected to photolysis by a medium-pressure mercury arc lamp (Phillips, 175W) with the globe removed.

DFT calculations were performed using the Gaussian 98 program system.[21] All equilibrium geometries were fully optimized with the BPW91 density functional (Becke exchange with Perdew and Wang correlation)[22,23] and 6-311+G(d) basis set for nitrogen and LANL2DZ pseudopotential for rhodium.[24−26] The relative energies of calculated species were corrected for zero-point energy. The harmonic vibrational frequencies were obtained analytically at the optimized structures.

Results

Infrared spectra are presented for reaction products of laser-ablated rhodium atoms with N_2 in solid neon, argon, and nitrogen. For comparison, the infrared spectra and structures of various rhodium and dinitrogen complexes are reproduced by theoretical calculations.

Neon Spectra. Figure 1 shows infrared spectra of laser-ablated rhodium codeposited with 0.4% N_2 in excess neon using very low laser energy, and the absorptions are listed in Table 1. Additional experiments were performed with 0.2 and 1% N_2 in neon to profile concentration dependence. Absorptions common to these experiments, namely, N_2, N_4^+, and N_3, have

10.1021/jp013527m CCC: $22.00
Published on Web 02/14/2002

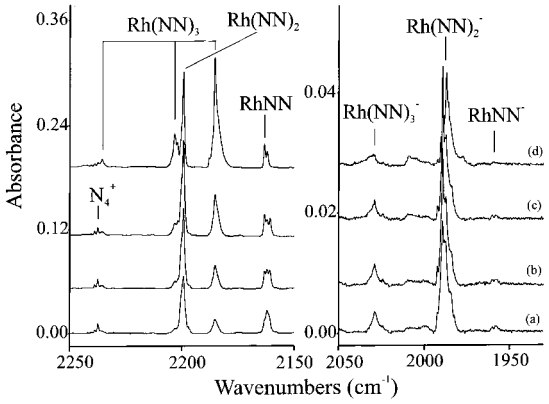

Figure 1. Infrared spectra in the 2250−2150 and 2050−1930 cm^{-1} regions for laser-ablated Rh atoms codeposited with N_2 in excess neon: (a) 0.4% N_2 in neon deposited at 4 K for 40 min, (b) after annealing to 8 K, (c) after annealing to 10 K, and (d) after annealing to 12 K.

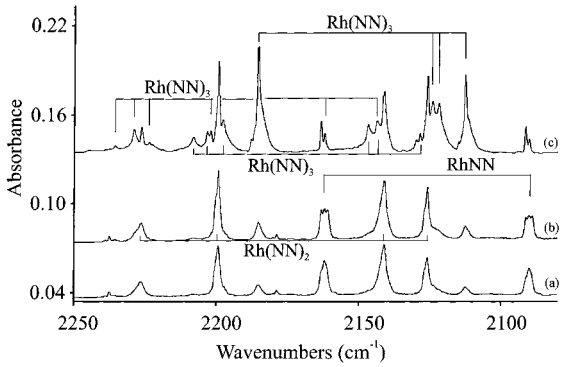

Figure 2. Infrared spectra in the 2250−2080 cm^{-1} region for laser-ablated Rh atoms codeposited with $^{14}N_2$ and $^{15}N_2$ mixture in excess neon: (a) 0.1% $^{14}N_2$ + 0.1% $^{15}N_2$ in neon deposited at 4 K for 60 min, (b) after annealing to 8 K, and (c) after annealing to 10 K.

been reported previously.[17,20,27−31] After deposition, a group of upper bands at 2235.6, 2203.3, 2199.3, 2185.2 and 2163.1 cm^{-1} and a group of lower bands at 2029.0, 1989.3, and 1957.4 cm^{-1} were observed. The $^{14}N_2 + {}^{15}N_2$ mixture samples gave isotopic distributions as shown in Figures 2 and 3. Different temperature annealing and wavelength range photolysis were done to characterize the absorptions. Briefly, $\lambda > 380$, 290, and 240 nm irradiations destroyed the 1957.4, 1989.3, and 2029.0 cm^{-1} bands, respectively. In addition, experiments were done with 0.02% CCl_4 added to 0.2% N_2 to serve as an electron trap in the neon matrix and the lower group bands were almost eliminated from the spectra. The lower group of bands can been assigned to anions.

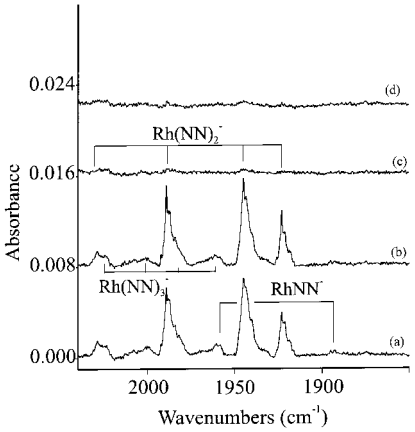

Figure 3. Infrared spectra in the 2050−1850 cm^{-1} region for laser-ablated Rh atoms codeposited with $^{14}N_2$ and $^{15}N_2$ mixture in excess neon: (a) 0.1% $^{14}N_2$ + 0.1% $^{15}N_2$ in neon deposited at 4 K for 60 min, (b) after annealing to 8 K, (c) after broadband photolysis for 10 min, and (d) after annealing to 10 K.

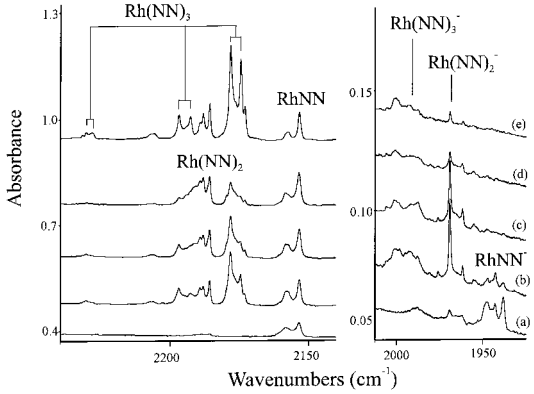

Figure 4. Infrared spectra in the 2240−2140 and 2010−1920 cm^{-1} regions for laser-ablated Rh atoms codeposited with N_2 in excess argon: (a) 0.3% N_2 in argon deposited at 4 K for 80 min, (b) after annealing to 20 K, (c) after 380 nm filter photolysis for 10 min, (d) after broadband photolysis for 10 min, and (e) after annealing to 35 K.

Argon Spectra. Several experiments were done in an argon matrix with 4 K deposition, which favored the stabilization of anion and other unstable species, and the spectra are shown in Figure 4 and the product absorptions are listed in Table 2. Different temperature annealing and wavelength range photolysis were done, and a $^{14}N_2 + {}^{15}N_2$ mixture sample was used to assign the absorptions as shown in Figure 5. It is noted that the chemistry of the species observed in the argon matrix is very similar to that of the neon counterparts.

TABLE 1: Absorptions (cm^{-1}) from Codeposition of Laser-Ablated Rh with N_2 in Excess Neon at 4 K

$^{14}N_2$	$^{15}N_2$	$^{14}N_2 + {}^{15}N_2$	$^{14}N/{}^{15}N$	assignment
2610.8				$Rh(NN)_3$
2237.4	2162.9	2265.9, 2037.4, 2178.8, 2162.9	1.0344	N_4^+
2235.6	2161.0	2235.6, 2228.8, 2223.6, 2202, 2161, 2143.5	1.0345	$Rh(NN)_3$
2203.3	2129.8	2208.1, 2203.2, 2197.7, 2146.7, 2143.5, 2129.8	1.0345	$Rh(NN)_3$
2199.3	2125.9	2199.3, 2140.9, 2125.9	1.0345	$Rh(NN)_2$
2185.2	2112.4	2185.2, 2124.1, 2121.9, 2112.6	1.0345	$Rh(NN)_3$
2163.1	2091.1	2163.1, 2091.1	1.0344	RhNN (site)
2162.0	2090.0	2162.0, 2090.0	1.0344	RhNN
2160.7	2088.9	2160.7, 2088.9	1.0344	RhNN (site)
2029.0	1961.1	2029.0, 2000.4, 1979.2, 1961.1	1.0346	$Rh(NN)_3^-$
1989.3	1923.5	1989.3, 1945.0, 1923.5	1.0342	$Rh(NN)_2^-$
1987.3	1921.3		1.0343	$Rh(NN)_2^-$ (site)
1957.4	1892.5	1957.4, 1892.5	1.0343	$RhNN^-$
1778.1	1718.6	1778.1, 1718.6	1.0346	$Rh_2(N_2)$

TABLE 2: Absorptions (cm^{-1}) from Codeposition of Laser-Ablated Rh with N_2 in Excess Argon at 4 K

$^{14}N_2$	$^{15}N_2$	$^{14}N_2 + ^{15}N_2$	$^{14}N/^{15}N$	assignment
2230.7	2156.5	*a*	1.0344	$Rh(NN)_3$
2228.4	2154.1	*a*	1.0345	$Rh(NN)_3$(site)
2196.8	2123.7	*a*	1.0344	$Rh(NN)_3$
2193.3	2120.1	*a*	1.0345	$Rh(NN)_3$(site)
2188.4	2115.2	2188.4, 2132.8, 2115.2	1.0346	$Rh(NN)_2$(site)
2185.9	2112.8	2185.8, 2128.9, 2112.8	1.0346	$Rh(NN)_2$
2178.4	2105.9	2178.4, 2142.8, 2133.6, 2113.7, 2105.9	1.0344	$Rh(NN)_3$
2173.5	2101.1	2173.5, 2140.8, 2129.3, 2111.3, 2101.1	1.0345	$Rh(NN)_3$(site)
2157.8	2086.2	2157.8, 2086.2	1.0343	Rh(NN)(site)
2153.5	2081.7	2153.4, 2081.7	1.0345	Rh(NN)
1993.2	1926.4	1993.3, 1964.3, 1947.4, 1926.4	1.0347	$Rh(NN)_3^-$(site)
1975.6	1909.8	1975.2, 1931.8, 1909.6	1.0345	$Rh(NN)_2^-$
1969.9	1904.2	1969.4, 1926.4, 1904.0	1.0345	$Rh(NN)_2^-$(site)
1958.9	1893.4	1958.1, 1893.0	1.0346	$Rh(NN)^-$
1954.5	1889.5	1954.4, 1889.5	1.0344	$Rh(NN)^-$(site)
1950.9	1885.9	1950.7, 1885.8	1.0345	$Rh(NN)^-$(site)
1762.3	1704.3	1762.2, 1703.7	1.0340	$Rh_2(N_2)$

[a] Region too congested to observe distinct absorptions.

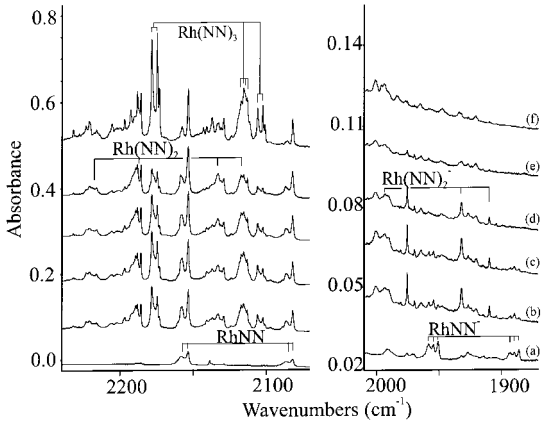

Figure 5. Infrared spectra in the 2240−2060 and 2010−1870 cm^{-1} regions for laser-ablated Rh atoms codeposited with $^{14}N_2 + ^{15}N_2$ in excess argon: (a) 0.2% $^{14}N_2$ + 0.2% $^{15}N_2$ in argon deposited at 4 K for 80 min, (b) after annealing to 20 K, (c) after annealing to 30 K, (d) after 380 nm filter photolysis for 10 min, (e) after broadband photolysis for 10 min, and (f) after annealing to 35 K.

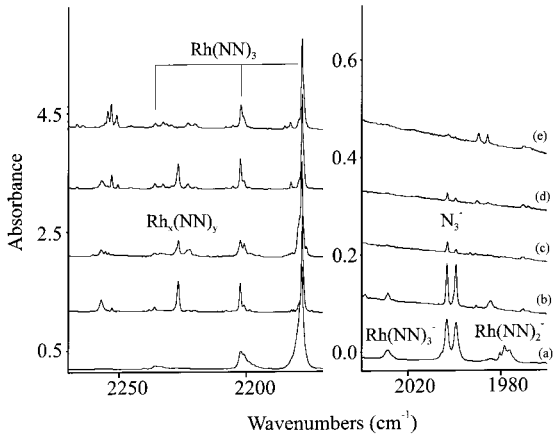

Figure 6. Infrared spectra in the 2270−2170 and 2040−1960 cm^{-1} regions for laser-ablated Rh atoms codeposited with pure N_2: (a) deposited at 4 K for 60 min, (b) after annealing to 30 K, (c) after broadband photolysis for 10 min, (d) after annealing to 32 K, and (e) after annealing to 35 K.

Nitrogen Spectra. A complementary series of nitrogen matrix experiments was done at 4 K using lower laser energy than previous laser-ablation work.[10] Very simple spectra were obtained as shown in Figure 6, and the absorptions are listed in Table 3. The lower region was dominated by a sharp 863.4 cm^{-1} feature,[10] and higher rhodium species were not observed.

Calculations. Four rhodium nitrogen complexes with end-on NN bond type, $Rh(NN)_x$ ($x = 1-4$), were calculated using the BPW91 functional, and doublet ground states, and were found for all four molecules at this level of theory. The Rh−NN complex has a linear structure with shortest Rh−N distance (1.864 Å) and longest N−N distance (1.134 Å) and the strongest interaction of dinitrogen with rhodium for the four neutral rhodium nitrogen complexes. The Rh−N bond distance increases, but the N−N bond length decreases from $Rh(NN)_2$ to $Rh(NN)_4$, indicating that interaction of rhodium atom with NN weakens as more NN ligands are coordinated to rhodium. The Rh−N bond length reaches 2.056 Å and the N−N bond decreases to 1.120 Å for $Rh(NN)_4$, showing very weak bonding of Rh and N_2 in this D_{2d} symmetry complex. Our DFT calculations find a linear $Rh(NN)_2$ complex and a T-shaped $Rh(NN)_3$ species. Parameters are given in Tables 4 and 5. Previous DFT calculations on RhNN found linear structures,[10,32] and one study of $Rh(NN)_2$ considered only the $^2B_2$ form,[32] which is 9.3 kcal/mol higher than the $^2\Sigma_g^+$ structure.

TABLE 3: Absorptions (cm^{-1}) from Codeposition of Laser-Ablated Rh with Pure N_2 at 4 K

$^{14}N_2$	$^{15}N_2$	$^{14}N_2 + ^{15}N_2$	$^{14}N/^{15}N$	assignment
2328.2	2250.4	2328.2, 2250.4	1.0346	N_2
2252.9	2177.8	*a*	1.0345	$Rh_x(NN)_y$
2236.1	2161.2	*a*	1.0346	$Rh(NN)_3$
2226.7	2152.5	*a*	1.0345	$Rh_x(NN)_y$
2202.4	2128.8	*a*	1.0346	$Rh(NN)_3$
2200.9	2127.5	*a*	1.0345	$Rh(NN)_3$(site)
2178.2	2105.7	2178.2, 2121.8, 2115.6, 2105.7	1.0344	$Rh(NN)_3$
2028.7	1961.0	*a*	1.0345	$Rh(NN)_3^-$
2003.3	1936.6	2003.3, 1966.5, 1947.8, 1936.6	1.0344	N_3^-
1999.4	1932.9	1999.4, 1964.8, 1936.2, 1932.9	1.0344	N_3^- (site)
1978.4	1912.2	1978.4, 1928.3, 1912.2	1.0346	$Rh(NN)_2^-$
1657.6	1603.4	1657.6, 1649.4, 1613.0, 1603.3	1.0337	N_3

[a] Region too congested to observe distinct absorptions.

The rhodium dinitrogen complex anions were computed at the same level to compare with the neutral counterparts. The $RhNN^-$ anion has a linear structure with a $^1\Sigma^+$ ground state and the Rh−N and N−N bond lengths are 1.783 and 1.158 Å, respectively, indicating the NN bond in rhodium nitrogen complexes elongates on electron attachment. Two isomers for $Rh(NN)_2^-$ were obtained; the bent C_{2v} structure with $^1A_1$

TABLE 4: Rhodium Nitrogen Complex States, Relative Energies, Geometries, and N−N Vibrational Frequencies, Calculated at the BPW91/6-311+G(d)/LANL2DZ Level

molecule	state	relative energy[a]	geometry (Å, deg)	N−N stretching[b]
RhNN ($C_{\infty v}$)	$^2\Delta$	0.0	RhN,1.864; NN,1.134; RhNN,180.0	2099.0 (394) 470.1 (12) 251.4 (7 × 2)
$RhNN^-$ ($C_{\infty v}$)	$^1\Sigma^+$	−28.5	RhN,1.783; NN,1.158; RhNN,180.0	1978.9 (824) 560.2 (0.2) 314.1 (13 × 2)
$Rh(NN)_2$ ($D_{\infty h}$)	$^2\Sigma_g^+$	0.0	RhN, 1.939; NN, 1.125; RhNN, 180.0	2148.6 (1217)[c] 2202.7 (0)
$Rh(NN)_2$ (C_{2v})	$^2B_2$	+9.3	RhN,1.949; NN,1.126; RhNN,175.0; NRhN,107.3	2132.1 (806) 2167.6 (113)
$Rh(NN)_2$ (C_{2v})	$^2A_1$	+63.6	RhN, 1.895; NN, 1.133, RhNN, 168.6; NRhN, 89.2	2006.6 (1138) 2091.2 (824)
$Rh(NN)_2^-$ (C_{2v})	$^1A_1$	−45.3	RhN,1.893; NN,1.145; RhNN,180.0; NRhN,159.1	2010.8 (2209) 2066.9 (42)
$Rh(NN)_2^-$ ($D_{\infty h}$)	$^3\Pi_u$	−20.6	RhN,1.932; NN,1.155; RhNN,180.0; NRhN,180.0	1923.3 (2859) 1963.7 (0)
$Rh(NN)_3$ (C_{2v})	$^2A_1$	0.0	RhN,1.985; RhN′,2.015; NN,1.122; NN′,1.121; RhNN,180.0; RhN′N′,180.0	2170.8 (992) 2176.4 (401) 2214.5 (18)
$Rh(NN)_3^-$ (D_{3h})	$^2A_1$	−52.9	RhN,1.960; NN,1.140; RhNN,180.0	2036.8 (1644 × 2)
$Rh(NN)_4$ (D_{2d})	$^2B_2$	0.0	RhN,2.056; NN,1.120; RhNN,180.0.0; RhN,151.1; NRhN′,93.6	2167.0 (153) 2181.1 (855 × 2) 2219.6 (0)
N_2 ($D_{\infty h}$)	$^1\Sigma_g^+$	0.0	NN, 1.107	2349.3 (0)

[a] kcal/mol. [b] Frequencies, cm^{-1} (intensities, km/mol). [c] Frequencies for 15−15-R-14−14 isotope are 2093.5 (916), 2184.2 (261) and for $Rh(15-15)_2$ isotope are 2076.0 (136), 2128.2 (0). Other frequencies are 410.4 (2 × 2), 401.6 (107), 396.8 (0), 282.1 (0 × 2), 52.4 (1 × 2).

TABLE 5: Dinitrogen Stretching Frequencies (cm^{-1}) and Infrared Intensities (km/mol) of Isotopic $Rh(NN)_3$ and $Rh(NN)_4$ Complexes Calculated at the BPW91/6-311+G(d)/LANL2DZ Level for Ground State Rhodium Nitrogen Complexes

molecule[a]	b_2	a_1	a_1
$Rh(^{14}NN)_2(^{14}NN)$	2170.8 (992)	2176.4 (401)	2214.5 (18)
$Rh(^{15}NN)_2(^{15}NN)$	2097.4 (926)	2102.8 (374)	2139.7 (16)
$Rh(^{14}NN)_2(^{15}NN)$	2170.8 (992)	2113.4 (367)	2203.5 (29)
$Rh(^{15}NN)_2(^{14}NN)$	2097.4 (926)	2196.0 (239)	2120.6 (174)
$Rh(^{14}NN, ^{15}NN)(^{14}NN)$[b]	2107.4 (659)	2174.9 (550)	2205.6 (165)
$Rh(^{14}NN, ^{15}NN)(^{15}NN)$[b]	2101.1 (565)	2121.7 (484)	2190.9 (304)

molecule[a]	b_2	e	e	a_1
$Rh(^{14}NN)_2(^{14}NN)_2$	2167.0 (153)	2181.1 (855)	2181.1 (855)	2219.6 (0)
$Rh(^{15}NN)_2(^{15}NN)_2$	2093.8 (143)	2107.4 (798)	2107.4 (798)	2144.6 (0)
$Rh(^{14}NN)_2(^{15}NN)_2$	2107.4 (798)	2111.1 (114)	2181.1 (855)	2201.5 (34)
$Rh(^{14}NN, ^{15}NN)(^{14}NN)_2$	2109.2 (459)	2172.2 (432)	2181.1 (855)	2212.4 (86)
$Rh(^{14}NN, ^{15}NN)(^{15}NN)_2$	2097.4 (276)	2107.4 (798)	2129.1 (384)	2193.2 (312)
$Rh(^{14}NN, ^{15}NN)(^{14}NN, ^{15}NN)_2$	2099.9 (408)	2121.4 (588)	2174.7 9567)	2204.9 (239)

[a] Mode symmetry for natural isotopic molecule. [b] Double statistical weight in 50% $^{14}N_2$ + 50% $^{15}N_2$ mixture.

symmetry is the ground state and the linear $D_{\infty h}$ structure $^3\Sigma_g^+$ state is 24.7 kcal/mol higher. The $Rh(NN)_3^-$ anion is predicted to have a $^1A_1$ ground state with D_{3h} symmetry. Similar structures were found in previous calculations[32] and for the carbonyl analogues.[11]

Discussion

RhNN. In the neon matrix, a strong band centered at 2162.0 cm^{-1} is assigned to the RhNN complex. This band appeared after sample deposition, split into sites on annealing, and shifted down to 2090.0 cm^{-1} with $^{15}N_2$ sample, giving a 1.0344 $^{14}N/^{15}N$ isotopic frequency ratio. The $^{14}N_2 + {}^{15}N_2$ experiment reveals a clear 2162.0 and 2090.0 cm^{-1} mixed isotopic doublet; hence, one NN submolecule is involved in these vibrations (note the matching site structure in Figure 2). Furthermore, the 2162.0 cm^{-1} band is the only nitrogen species observed in other rhodium experiments when N_2 is present as a trace impurity. The NN stretching mode for RhNN in the argon matrix is red-shifted 8.5 cm^{-1} relative to neon, and the same isotopic frequency ratio is found. This assignment is in agreement with previous work.[10,15] The RhCO complex exhibited a similar 14.9 cm^{-1} neon-to-argon red shift.[11] The 2162.0 cm^{-1} neon matrix frequency for RhNN is 91 ± 5 cm^{-1} lower than for N_2 chemisorbed on metallic rhodium,[1,2,5] which suggests a stronger interaction with a single atom. The same is found for platinum.[17]

The DFT calculation for this complex reproduces the experimental values very well; the calculated N−N stretching frequency is 46 cm^{-1} lower than the neon matrix value, and the calculated $^{14}N/^{15}N$ isotopic ratio is 1.0350, very close to the observed value of 1.0344. Although our BPW91 calculation found a slightly bent $^2A'$ ground state for RhNN, a B3LYP calculation probably correctly predicts the ground state as $^2\Delta$.[32] The DFT frequencies are usually slightly higher than observed values;[33] however, the BP86 frequency calculated for $^2\Delta$ RhCO is 19 cm^{-1} lower than the neon matrix observation.[11]

$Rh(NN)_2$. A strong, sharp band at 2199.3 cm^{-1} increases on early annealing, but holds while the 2185.2 cm^{-1} band overtakes on final annealing in solid neon. The $^{15}N_2$ counterpart at 2125.9 cm^{-1} gives the isotopic ratio of 1.0345. In the $^{14}N_2 + {}^{15}N_2$ experiment two new $^{14}N_2Rh^{15}N_2$ bands at 2140.9 and 2226.2 cm^{-1} were observed in addition to the pure $^{14}N_2$ and $^{15}N_2$ bands (Figure 2). The intermediate 2140.9 cm^{-1} band occurs much lower than the median of $Rh(^{14}N_2)_2$ at 2199.3 cm^{-1} and $Rh(^{15}N_2)_2$ at 2125.9 cm^{-1} with approximately the intensity of the pure isotopic bands; however, the new 2226.2 cm^{-1} band is just above the mode for $Rh(^{14}N_2)_2$ at 2199.3 cm^{-1}. The reduced intensity and displacement of the intermediate component are due to coupling of the "symmetric" and "antisymmetric" modes in the $^{14}N_2Rh^{15}N_2$ molecule. The infrared intensity of the "symmetric" mode is enhanced by this coupling, so the 2226.2 cm^{-1} band is much stronger than pure isotopic N−N symmetric modes, which are not observed. Similar behavior was found for $Pt(NN)_2$.[17] Clearly, the 2199.3 cm^{-1} band can be assigned to the antisymmetric N−N stretching mode of $Rh(NN)_2$.

Experiments with 0.2% N_2 in argon on a 5 K substrate give the representative spectra shown in Figure 4. A strong band at 2185.9 cm^{-1} and satellite at 2188.4 cm^{-1} are due to the

antisymmetric N−N stretching mode of $Rh(NN)_2$. The strong band shows the same mixed $^{14}N_2 + {}^{15}N_2$ isotopic distributions in argon as in the neon experiments, which indicates the $Rh(NN)_2$ identification. The argon matrix band is 13.4 cm^{-1} below the neon matrix band and in agreement with the previous assignment.[15]

The $Rh(NN)_2$ assignment is strongly supported by the DFT frequency calculations presented in Table 4. The N−N antisymmetric mode for this linear complex is predicted at 2148.6 cm^{-1}, only 57.7 cm^{-1} lower than the neon matrix value. The predictions of two modes for $^{14}N_2Rh^{15}N_2$ at 2093.5 and 2184.2 cm^{-1} with 3.5 to 1.0 relative intensity are 47.4 and 42.0 cm^{-1} lower than the neon matrix bands and match the experimental relative band intensity (3.5 to 1.0, Figure 2b). It should be noted that the early thermal work suggested that $Rh(NN)_2$ is linear based on only one absorption at 2188 cm^{-1} in solid argon.[15] The $Rh(I)(N_2)_2$ species on supported Y zeolite absorbs at 2243 and 2217 cm^{-1} and on alumina at 2188 cm^{-1}.[4,8] Although these bisdinitrogen species are bent, comparison with our 2199.3 cm^{-1} observation of linear $Rh(NN)_2$ is informative as the calculated antisymmetric frequency difference between bent and linear forms is only 19 cm^{-1} (Table 4). McKee and Worley report a much larger 154 cm^{-1} increase for the $^3B_2$ cation over the $^2B_2$ neutral.[32] This strongly suggests that the supported $Rh(I)(N_2)_2$ species frequencies are not high enough for $I = +1$ although there may be a small fractional positive charge on the supported Rh center. A similar interpretation has been offered for the supported $Rh(I)(CO)_2$ species.[11,12] Our new neon matrix results and calculations suggest strongly that the $Rh(NN)_2$ complex is linear. The symmetric N−N stretching mode should be in the clean 2240−2260 cm^{-1} region, and the failure to observe this band again evidences the linear structure.

$Rh(NN)_3$. In neon experiments a new band at 2185.2 cm^{-1} increased on annealing at 10 K, decreased on full arc photolysis, and increased 3-fold on annealing to 12 K. A medium intensity band at 2203.3 cm^{-1} and a very weak absorption at 2235.6 cm^{-1} track the strong band at 2185.2 cm^{-1}. These three bands shift to 2161.0, 2129.8, and 2112.4 cm^{-1}, respectively, in the $^{15}N_2$ experiment with exactly the same 1.0345 $^{14}N/^{15}N$ isotopic frequency ratio. The $^{14}N_2 + {}^{15}N_2$ mixed isotopic experiments give a very complicated distribution pattern for each fundamental as listed in Table 1 and shown in Figure 2; the pure $^{14}N_2$ and $^{15}N_2$ bands at 2185.2 and 2112.4 cm^{-1} are dominant and medium and weak mixed isotopic bands are produced. The argon matrix counterparts for these bands are at 2178.4, 2196.8, and 2230.7 cm^{-1}, respectively, which are slightly red shifted relative to neon values, but show the same annealing and photolysis behavior. Rhodium atoms codeposited with pure nitrogen molecules yielded three bands at 2179.3 (strong), 2202.4 (medium), and 2236.1 (weak) cm^{-1} in this range (Figure 6). The relative intensities of these three bands are essentially the same as the modes observed in neon and argon matrices. However, the bands decreased in concert on stepwise annealing and disappeared on broadband photolysis, and more complicated $Rh_x(NN)_y$ complexes appeared.

Both $Rh(NN)_3$ and $Rh(NN)_4$ are considered as possible sources for these three N−N stretching modes. Here the theoretical frequency calculations are extremely helpful because the isotopic patterns are complicated. The $Rh(NN)_3$ complex is predicted to be T-shaped with a $^2A_1$ ground state, and three N−N stretching modes are obtained at 2170.8 cm^{-1} (antisymmetric NN−Rh−NN), 2214.5 cm^{-1} (symmetric NN−Rh−NN), and 2176.4 cm^{-1} (symmetric Rh−N′N′). The isotopic frequency calculations for these modes are listed in Table 5. The antisymmetric stretching with the strongest intensity is predicted to show effectively a "quartet" with (992+992):659 × 2:565 × 2:(926+926) or approximately 2:1:1:2 relative intensities; however, the other two modes are calculated to have six-band profiles. As compared with experimental observations, these calculated results agree extremely well. First, the three fundamentals are predicted low by 21 ± 6 cm^{-1} with 50/20/1 relative intensities, in excellent agreement with the observed 40/12/2 relative intensities. Second, the observed mixed isotopic profiles (Figure 2) match the calculated frequencies and intensities with similar accuracy (Table 5). Accordingly, the above three-band sets are assigned to $Rh(NN)_3$. In addition, the weak 2610.8 cm^{-1} band is probably a combination band involving the strong N−N fundamental and the a_1 Rh−$(NN)_2$ stretching mode; the 425.6 cm^{-1} difference is near the 400 cm^{-1} calculated value for this mode. It is now clear that the previous bands assigned to $Rh(NN)_4$ are in fact due to $Rh(NN)_3$, and the characterizations of $Rh(NN)_3$ and $Rh(NN)_4$ in that work[15] are not correct, although a 2196 cm^{-1} band was assigned to the tris complex.

The DFT/BPW91 calculation predicts a $^2B_2$ ground state for the $Rh(NN)_4$ complex in D_{2d} symmetry. The calculated isotopic frequencies are listed in Table 5, and the most intense mode is doubly degenerate at 2181.1 cm^{-1}. This mode should exhibit a broad doublet distribution with mixed $^{14}N_2 + {}^{15}N_2$ isotopic substitution; however, other modes are predicted to have less than 10% of this intensity. Therefore the observed spectrum cannot be assigned to the $Rh(NN)_4$ molecule.

In the early rhodium dinitrogen complex investigation, the dominant bands at 2177 cm^{-1} in solid argon and 2179/2203 cm^{-1} in solid nitrogen were unfortunately assigned to $Rh(NN)_4$ with D_{2d} symmetry based on comparison with analogous $Ni(NN)_4$ spectra and force constant calculations.[15] Mixed isotopic frequencies for these bands were observed but believed too complicated to interpret. The present isotopic frequencies and DFT calculations require assignment of this species as $Rh(NN)_3$ and rule out the observation of $Rh(NN)_4$. Unlike $Rh(CO)_4$, the $Rh(NN)_4$ complex does not appear to be formed, even in solid dinitrogen.

Bonding Considerations. This assignment is also supported by calculations of energy changes for the formations of $Rh(NN)_x$ ($x = 1-4$). Reactions 1, 2, and 3 are exothermic by 28.4, 19.4 and 16.9 kcal/mol at the BPW91 level, respectively, but reaction 4 is much less exothermic, and hence, the thermodynamic driving force to give $Rh(NN)_4$ is limited.

$$Rh + NN \rightarrow RhNN(^2\Delta) \qquad \Delta E = -28.4 \text{ kcal/mol} \quad (1)$$

$$Rh(NN) + NN \rightarrow Rh(NN)_2\,(^3\Sigma_g^+) \qquad \Delta E = -19.4 \text{ kcal/mol} \quad (2)$$

$$Rh(NN)_2 + NN \rightarrow Rh(NN)_3\,(^2A_1) \qquad \Delta E = -16.9 \text{ kcal/mol} \quad (3)$$

$$Rh(NN)_3 + NN \rightarrow Rh(NN)_4(^2B_2) \qquad \Delta E = -0.9 \text{ kcal/mol} \quad (4)$$

In contrast, energy changes for the analogous carbonyls are more exothermic, hence the carbonyls are more stable, based on the conventional wisdom that CO is a stronger σ donor and π acceptor than the isoelectronic N_2 molecule.[34] The BPW91/6-311+G(d)/LANL2DZ energy changes for reactions 5−8 are considerably higher than for their N_2 analogues. Our BPW91 energies may be too high as reaction 5 is computed to be exothermic by only 42 kcal/mol at the CASMCSCF level of

theory.[35] The carbonyl structures and frequencies are close to values reported earlier using the BP86 functional.[11]

$$Rh + CO \rightarrow RhCO\ (^2\Delta) \qquad \Delta E = -59.1\ \text{kcal/mol} \quad (5)$$

$$RhCO + CO \rightarrow Rh(CO)_2\ (^2\Sigma_g^+) \qquad \Delta E = -37.8\ \text{kcal/mol} \quad (6)$$

$$Rh(CO)_2 + CO \rightarrow Rh(CO)_3\ (^2A_1) \qquad \Delta E = -35.5\ \text{kcal/mol} \quad (7)$$

$$Rh(CO)_3 + CO \rightarrow Rh(CO)_4\ (^2B_2) \qquad \Delta E = -22.1\ \text{kcal/mol} \quad (8)$$

The greater stability of carbonyl complexes relative to dinitrogen complexes is clearly illustrated in a recent thermochemical investigation using gaseous Ni^+ cations.[18] The $NiCO^+$ and $NiNN^+$ dissociation energies were found to be 41.6 and 26.6 ± 2.5 kcal/mol, respectively, and the $(CO)_3Ni^+-CO$ and $(N_2)_3Ni^+-N_2$ dissociation energies were 17.3 ± 0.7 and 10.1 ± 2 kcal/mol, respectively. The fourth ligand is clearly bound less strongly than the first and N_2 is a weaker ligand than CO at all coordination numbers.[18] Thus, the gas-phase studies and theoretical calculations both show that N_2 is a weaker ligand than CO, as expected.

It is interesting to compare the geometries, frequencies, and natural bond orbital charges for RhNN and RhCO. Both molecules are predicted to be linear, with $^2\Delta$ ground states, and the N−N bond in RhNN is elongated 0.027 Å from free NN, whereas the CO bond length in RhCO is increased 0.024 Å compared to free CO. In a neon matrix the NN stretching frequency in RhNN is red shifted 166 cm^{-1} from free NN; however, the CO stretching mode in RhCO shows a 118 cm^{-1} red shift from free CO. These results suggest more electron flow to NN from Rh through back-donation than with CO in RhCO, although CO is believed to be the stronger ligand in the general case.[34] Further comparisons can be made between the simple RhCO and RhNN complexes using the calculated natural bond orbital charges[21] Rh (+0.065) C (+0.389) O (−0.455) and Rh (+0.208) N (−0.160) N (−0.048). These charges show that Rh is more positive in RhNN, which is consistent with slightly greater π back-donation to N_2 in RhNN, in contrast to what is normally expected, although RhCO is overall more strongly bound than RhNN.

A small difference is found between the carbonyl frequencies in $Rh(CO)_{1-4}$ and N−N frequencies in $Rh(NN)_{1-4}$. In the carbonyl case, the strong neon matrix fundamentals[11] fall in the 2031−2018 cm^{-1} range around RhCO at 2022 cm^{-1}, but in the dinitrogen case the strong $Rh(NN)_{2,3}$ fundamentals at 2199 and 2185 cm^{-1} are less red shifted than RhNN at 2162 cm^{-1}. Calculated ligand stretching frequencies, including the unobserved $Rh(NN)_4$ molecule exhibit the same relationship: the average calculated C−O frequencies for $Rh(CO)_{2,3,4}$ (2022, 2011, 2008 cm^{-1}) are slightly above the RhCO value (2004 cm^{-1}),[11] but the average calculated N−N frequencies for $Rh(NN)_{2,3,4}$ (2176, 2187, 2187 cm^{-1}) are substantially higher than the RhNN value (2099 cm^{-1}). Hence, any advantage RhNN appears to enjoy in π back-donation is lost in the higher dinitrogen complexes probably owing to less favorable orientation, which accounts for the weaker bonds in $Rh(NN)_4$. On the other hand, σ donation suffers no such loss with structure, and $Rh(CO)_4$ is correspondingly more stable.

$Rh(NN)^-_{1,2,3}$. A weak band observed on deposition of rhodium and nitrogen in neon at 1989.3 cm^{-1} sharpens on sample annealing and $\lambda > 380$ nm photolysis but disappears on $\lambda > 290$ nm photolysis. Doping with CCl_4 to trap electrons from the ablation process[11,12,16,17] eliminates the 1989.3 cm^{-1} band, which strongly suggests the anion assignment. A dominant triplet profile with a very weak upper band is obtained in $^{14}N_2 + {}^{15}N_2$ experiments, much like that observed for $Rh(NN)_2$, indicating that two equivalent NN submolecules are involved in this vibration. The weak upper band is due to the symmetric mode of $^{14}N_2Rh^{15}N_2^-$. The 1983.9 cm^{-1} band is assigned to the antisymmetric N−N stretching vibration of the $Rh(NN)_2^-$ anion. A similar band was observed in the argon matrix at 1975.6 cm^{-1} with a site at 1969.9 cm^{-1}. This band again shows a triplet distribution in $^{14}N_2 + {}^{15}N_2$ experiments, and a weak higher symmetric mode for $^{14}N_2Rh^{15}N_2^-$ tracks together. The 1975.6 cm^{-1} argon band exhibited the analogous behavior compared to the 1989.3 cm^{-1} neon band on sample annealing, photolysis, and CCl_4 doping experiments. The 13.7 cm^{-1} argon-to neon matrix shift is slightly larger than that found for neutral $Rh(NN)_2$, indicating a stronger argon matrix effect for ionic species as expected. The counterpart band of $Rh(NN)_2^-$ was also observed at 1976.2 cm^{-1} with a site at 1978.2 cm^{-1} in pure nitrogen.

The $Rh(NN)_2^-$ anion assignment is further confirmed by DFT calculations. A strong antisymmetric mode at 2010.8 cm^{-1} (2209 km/mol) is predicted for $Rh(NN)_2^-$, which is only about 21.5 cm^{-1} higher than the neon matrix value. The symmetric mode for this molecule at 2066.9 cm^{-1} is too weak (42 km/mol) to be observed, but the predicted N−N stretching vibrations for $(^{14}N_2Rh^{15}N_2)^-$ at 1960.3 cm^{-1} (1713 km/mol) and 2048.5 cm^{-1} (463 km/mol) match the experimental values very well.

In solid neon the very weak band at 2029.0 cm^{-1} can be assigned to $Rh(NN)_3^-$. The 2029.0 cm^{-1} band decreased on sample annealing, decreased on $\lambda > 380$ nm photolysis, and disappeared on $\lambda > 240$ nm photolysis. The 3:1:1:3 isotopic distribution was obtained in $^{14}N_2 + {}^{15}N_2$ experiments indicates that three equivalent NN subunits are involved in this molecule, and $Rh(NN)_3^-$ is the best candidate. Doping CCl_4 in the N_2/Ne sample with 1/10 concentration of N_2 eliminated this band, suggesting anion species identification. The very weak band at 1993.2 cm^{-1} in the argon matrix is due to the $Rh(NN)_3^-$ complex. The calculations for $Rh(NN)_3^-$ predict a $^1A_1$ ground state with D_{3h} symmetry, a degenerate frequency at 2036.8 cm^{-1}, and isotopic distributions which agree with the experimental values.

The 1957.4 cm^{-1} band in solid neon shows similar behavior with $Rh(NN)_3^-$ on sample deposition, annealing, and doping with CCl_4. In addition the yield of this species in neon is much less than $Rh(NN)_3^-$, and the band is destroyed on $\lambda > 380$ nm photolysis, indicating this is the most unstable of the three anions. The weak doublet observed in $^{14}N_2$ and $^{15}N_2$ experiments and very close 1978.9 cm^{-1} DFT prediction support the $Rh(NN)^-$ assignment. The absorption of $RhNN^-$ was observed at 1950.9 cm^{-1} with two sites at 1954.5 and 1958.9 cm^{-1} in the argon matrix where this band appeared as the dominant ionic species on sample deposition since argon freezes more quickly and limits diffusion and reaction better than neon. However, this band decreased in intensity about 90% on annealing to 25K, and the bands due to $Rh(NN)_2^-$ and $Rh(NN)_3^-$ increased in great quantity (Figure 4), indicating that $Rh(NN)_2^-$ and $Rh(NN)_3^-$ are more stable and can be formed from $Rh(NN)^-$.

The ground states of $Rh(NN)_2^-$ and $Rh(NN)_3^-$ were calculated to be 45.3 and 52.7 kcal/mol lower in energies than the counterpart neutral molecules, hence the electron affinities of $Rh(NN)_2$ and $Rh(NN)_3$ are expected to be 2.0 to 2.3 ev. However

the electron affinity of RhNN is estimated to be 1.3 ev, which is about 1 ev lower than that of $Rh(NN)_2$ and $Rh(NN)_3$. These theoretical electron affinity estimations are in general agreement with our photolysis experiments where $\lambda > 380$, 290, 240 nm, respectively, were required to destroy the $Rh(NN)_{1,2,3}^-$ anions. As shown in Figure 1, the intensity ratio of neutral $Rh(NN)_2$ to RhNN is approximately 2:1 in neon after sample deposition, but the intensity of $Rh(NN)_2^-$ is much stronger than $Rh(NN)^-$ (about 50:1). Although the electron affinity of $Rh(NN)_3$ is close to that for $Rh(NN)_2$, the band due to $Rh(NN)_3^-$ is weak because the neutral $Rh(NN)_3$ complex is produced in low yield on sample deposition.

$Rh_2(N_2)$. Citra and Andrews observed a weak band to appear at 1763.7 cm^{-1} on late annealing of argon/Rh/N_2 samples.[10] Mixed isotopic data verified the participation of a single N_2 molecule. This product was also observed in pure nitrogen where one $^{14}N^{15}N$ component indicated two symmetry equivalent N atoms. Our spectra are not complicated by the presence of RhNO, and the bands appear on annealing at 1762.3 and 1704.3 cm^{-1} for more dilute $^{14}N_2$ and $^{15}N_2$ in solid argon almost the same as reported previously. Mixed $^{14}N_2+^{15}N_2$ gives only a pure isotopic doublet. In our neon experiments the bands are observed at 1778.1 and 1718.6 cm^{-1} on sample deposition.

The present observations support the earlier identification of this product as a side-bound N_2 species. Earlier calculations showed that a side-bound $Rh_2(N_2)$ parallelogram structure is the most likely explanation for these absorptions.[10] This is of considerable interest as a side-bound dinitrogen complex and suggests that under the proper conditions N_2 can bind sideways to rhodium clusters. On higher annealing the diffusion and further reaction 9 of rhodium can occur with the primary RhNN complex.

$$RhNN + Rh \rightarrow Rh_2(N_2) \qquad (9)$$

Conclusions

Rhodium atoms react with N_2 on condensation in excess neon, argon and dinitrogen to form $Rh(NN)_x$ ($x = 1-3$) complexes and $Rh(NN)_x^-$ ($x = 1-3$) anions, which are identified by $^{15}N_2$ and $^{14}N_2 + {}^{15}N_2$ isotopic substitution on the observed fundamental frequencies. The vibrational frequencies and isotopic ratios are reproduced very well by BPW91 density functional calculations. The RhNN complex absorbs at 2162.0 cm^{-1} in solid neon, which is 91 ± 5 cm^{-1} lower than N_2 chemisorbed on metallic rhodium;[1,2,5] apparently dinitrogen interacts more strongly with a single Rh atom than on the metallic surface. The linear $Rh(NN)_2$ complex is characterized by strong antisymmetric N−N fundamentals for the pure $^{14}N_2$ and $^{15}N_2$ isotopic species and two N−N stretching modes for $(^{14}N_2)Rh(^{15}N_2)$ with 3.5 to 1.0 relative intensity accurately predicted by DFT. The T-shaped $Rh(NN)_3$ complex is identified from the match of observed and calculated values for three fundamentals for six isotopic molecules. The BPW91 frequencies are systematically 8−22 cm^{-1} high for the three $Rh(NN)_x^-$ anions but 15−66 cm^{-1} low for the three $Rh(NN)_x$ complexes relative to neon matrix observations. The $Rh(NN)_4$ complex, which is predicted to be very weakly bound, is not observed, and the bands assigned previously[15] to $Rh(NN)_4$ are here reassigned to $Rh(NN)_3$. This is one of several examples where N_2 complex stoichiometry falls short of the CO counterparts,[16,17] which can be attributed to the weaker binding of N_2 as a ligand. Similar iridium experiments were complicated by metal aggregation, but it appears that iridium is less reactive than rhodium with dinitrogen although the association reactions are calculated to be more exothermic.[36] Finally, the characterization of a side-bonded $Rh_2(N_2)$ species is supported by observation under the present more dilute matrix conditions.

Reactions of metal atoms with N_2 in excess neon, argon, and nitrogen are complementary. More reagent diffusion on condensation in neon relative to argon favors the formation of higher complexes, which are dominant in pure nitrogen. Finally, deposition of argon and nitrogen at 4 K results in better matrix isolation than deposition at 8 or 10 K.

Acknowledgment. We gratefully acknowledge support from N.S.F. Grant CHE 00-78836 and computer time from the San Diego Supercomputer Center.

References and Notes

(1) Wang, H. P.; Yates, J. T., Jr. *J. Phys. Chem.* **1984**, *88*, 852. Yates, J. T., Jr.; Haller, H. L. *J. Phys. Chem.* **1984**, *88*, 4660.
(2) Wey, J. P.; Burkett, H. D.; Neely, W. C.; Worley, S. D. *J. Am. Chem. Soc*. **1991**, *113*, 2919. Wey, J. P.; Neely, W. C.; Worley, S. D. *J. Phys. Chem.* **1991**, *95*, 8879. Wey, J. P.; Worley, C. D.; Neely, W. C.; Worley, S. D. *J. Phys. Chem.* **1992**, *96*, 7088.
(3) Ballinger, T. H.; Yates, J. T., Jr. *J. Am. Chem. Soc*. **1992**, *114*, 10074.
(4) Miessner, H. *J. Am. Chem. Soc.* **1994**, *116*, 11522.
(5) Pei, Z.; Fang, T. H.; Worley, S. D. *J. Phys. Chem*. **1995**, *99*, 3663.
(6) Wong, J. C. S.; Yates, J. T., Jr. *J. Phys. Chem*. **1995**, *99*, 12640.
(7) Wovchko, E. A.; Yates, J. T., Jr. *J. Am. Chem. Soc*. **1995**, *117*, 12557.
(8) Wovchko, E. A.; Yates, J. T., Jr. *J. Am. Chem. Soc*. **1996**, *118*, 10250.
(9) Citra, A.; Andrews, L. *J. Phys. Chem. A* **1999**, *103*, 7773 (Rh + O_2).
(10) Citra, A.; Andrews, L. *J. Phys. Chem. A* **1999**, *103*, 3410 (Rh + N_2).
(11) Zhou, M. F.; Andrews, L. *J. Phys. Chem. A* **1999**, *103*, 7773 (Rh + CO) and references therein.
(12) Zhou, M. F.; Andrews, L. *J. Am. Chem. Soc.* **1999**, *121*, 9171 (Rh + CO).
(13) Citra, A.; Andrews, L. *J. Am. Chem. Soc*. **2000**, *104*, 11897 (Rh + NO).
(14) Zehr, R.; Solodukhin, A.; Hayne, B. C.; French, C.; Harrison, I. *J. Phys. Chem. B* **2000**, *104*, 3094 and references therein.
(15) Ozin, G. A.; Vander Voet, A. *Can. J. Chem*. **1973**, *51*, 3332.
(16) Liang, B.; Zhou, M. F.; Andrews, L. *J. Phys. Chem. A* **2000**, *104*, 3905.
(17) Citra, A.; Wang, X.; Bare, W. D.; Andrews, L. *J. Phys. Chem. A* **2001**, *105*, 7799 (Pt + N_2). Wang, X.; Citra, A.; Andrews, L. Unpublished results (Pd + N_2).
(18) Khan, F. A.; Steele, D. L.; Armentrout, P. B. *J. Phys. Chem*. **1995**, *99*, 7819.
(19) Burkholder, T. R.; Andrews, L. *J. Chem. Phys*. **1991**, *95*, 8697.
(20) Hassanzadeh, P.; Andrews, L. *J. Phys. Chem*. **1992**, *96*, 9177.
(21) Frisch, M. J.; Trucks, G. W.; Schlegel, H. B.; Scuseria, G. E.; Robb, M. A.; Cheeseman, J. R.; Zakrzewski, V. G.; Montgomery, J. A., Jr.; Stratmann, R. E.; Burant, J. C.; Dapprich, S.; Millam, J. M.; Daniels, A. D.; Kudin, K. N.; Strain, M. C.; Farkas, O.; Tomasi, J.; Barone, V.; Cossi, M.; Cammi, R.; Mennucci, B.; Pomelli, C.; Adamo, C.; Clifford, S.; Ochterski, J.; Petersson, G. A.; Ayala, P. Y.; Cui, Q.; Morokuma, K.; Malick, D. K.; Rabuck, A. D.; Raghavachari, K.; Foresman, J. B.; Cioslowski, J.; Ortiz, J. V.; Stefanov, B. B.; Liu, G.; Liashenko, A.; Piskorz, P.; Komaromi, I.; Gomperts, R.; Martin, R. L.; Fox, D. J.; Keith, T.; Al-Laham, M. A.; Peng, C. Y.; Nanayakkara, A.; Gonzalez, C.; Challacombe, M.; Gill, P. M. W.; Johnson, B.; Chen, W.; Wong, M. W.; Andres, J. L.; Gonzalez, C.; Head-Gordon, M.; Replogle, E. S.; Pople, J. A. *Gaussian 98*, Revision A.6; Gaussian, Inc.: Pittsburgh, PA, 1998.
(22) Perdew, J. P. *Phys. Rev. B* **1986**, *33*, 8822.
(23) Becke, A. D. *J. Chem. Phys*. **1993**, *98*, 5648.
(24) Krishnan, R.; Binkley, J. S.; Seeger, R.; Pople, J. A. *J. Chem. Phys.* **1980**, *72*, 650.
(25) Wadt, W. R.; Hay, P. J. *J. Chem. Phys.* **1985**, *82*, 284.
(26) Hay, P. J.; Wadt, W. R. *J. Chem. Phys.* **1985**, *82*, 299.
(27) Tian, R.; Facelli, J. C.; Michl, J. *J. Phys. Chem.* **1988**, *92*, 4073.
(28) Thompson, W. E.; Jacox, M. E. *J. Chem. Phys*. **1990**, *93*, 3856.
(29) Chertihin, G. V.; Andrews, L.; Neurock, M. *J. Phys. Chem*. **1996**, *100*, 14609. (Fe+N_2).
(30) Andrews, L.; Citra, A.; Chertihin, G. V.; Bare, W. D.; Neurock, M. *J. Phys. Chem. A* **1998**, *102*, 2561. (Co, Ni + N_2)
(31) Kushto, G. P.; Souter, P. F.; Chertihin, G. V.; Andrews, L. *J. Chem. Phys.* **1999**, *110*, 9020. (Ti, Zr, Hf + N_2)

(32) McKee, M. L.; Worley, S. D. *J. Phys. Chem. A* **1997**, *101*, 5600.
(33) Bytheway, I.; Wong, M. W. *Chem. Phys. Lett.* **1998**, *282*, 219.
(34) Pelikan, P.; Boca, R. *Coord. Chem. Rev.* **1983**, *55*, 55.
(35) Dai, D.; Balasubramanian, K. *J. Chem. Phys.* **1994**, *101*, 2148.
(36) Wang, X.; Citra, A.; Andrews, L. unpublished results (Ir + N_2).